Chemotactic encounters between bacteria and phytoplankton – the stakes are high for encounters with small phytoplankton.

Riccardo Foffi[a], **Douglas R. Brumley**[b], **François Peaudecerf**[c], **Roman Stocker**[a], **and Jonasz Słomka**[a,1]

This manuscript was compiled on January 19, 2024

Chemotaxis, the ability to navigate along chemical gradients, enables motile bacteria to increase encounter rates with symbiotic partners such as phytoplankton cells. However, it remains unclear how strongly chemotactic encounters depend on the bacterial strategy employed to detect noisy and spatially confined gradients around phytoplankton of different sizes. Here, we compute analytically and numerically an upper bound on the chemotactic index, a dimensionless number that measures the increase in encounter rate with a phytoplankton cell due to chemotaxis over random motility alone. We find that chemotaxis potentially strongly enhances the efficiency of searches for small phytoplankton, owing to the ballistic nature of the encounter for those cells, but the magnitude of the chemotactic index is very sensitive to the bacterial ability to detect spatially confined gradients. For example, in productive waters, chemotaxis can decrease the search times of bacteria for micron-sized picophytoplankton by more than ten-fold, from days to a few hours. Still, this benefit of chemotaxis is easily erased – reducing by half the phytoplankton radius or doubling the bacterial swimming speed renders gradients undetectable. For larger phytoplankton (radius $\sim 30\,\mu$m), the decrease in the search time is more moderate, from a month to a week, and depends gently on gradient detection. Thus, engaging chemotaxis in interactions with small phytoplankton is a high-stakes game for bacteria: the potential payoff is large, but it changes abruptly with bacterial ability to sense gradients, a scenario that may promote a diversity of chemotactic strategies.

encounter rates | chemotaxis | bacteria-phytoplankton interactions | microbial ecology

Significance Statement

Swimming bacteria search for phytoplankton to exchange metabolites, which control nutrient cycling in the ocean. Chemotaxis can accelerate the search by navigating bacteria along gradients of chemicals exuded by phytoplankton. However, successful navigation requires bacterial detection of noisy gradients, yet the type of noise depends on phytoplankton size. Detection fails when gradients are too flat (large phytoplankton) or too spatially confined (small phytoplankton). We computed an upper bound on chemotaxis's advantage for different phytoplankton size classes and found that chemotaxis offers the largest reductions in search time for small phytoplankton. However, the advantage sensitively relies on bacteria's chemotactic strategy. Chemotactic encounters with small phytoplankton are thus a high-stakes game that may promote a diversity of size-dependent chemotactic strategies.

Chemotaxis, the ability of bacteria to navigate chemical gradients and reach proximity with phytoplankton cells, can be crucial for establishing symbiotic relationships and favoring metabolic exchanges which lie at the heart of oceanic carbon cycles (1–3). In the water column, phytoplankton cells generate complex chemical landscapes by leaking dissolved organic compounds which can be strong attractants for bacteria (4–6). The composition of marine phytoplankton communities, which can span two orders of magnitude in cell size, from $\sim 0.5\,\mu$m to hundreds of microns (7), exposes bacteria to gradients on a wide range of scales.

Bacterial chemotaxis operates by sensing temporal changes in the concentration of chemoattractant compounds and biasing bacterial motion towards regions where these chemoattractant concentrations are higher (8, 9). Based on a molecule counting process, chemotaxis is inherently subject to noise (10, 11), especially at the low attractant concentrations typical of oceanic environments (12). The limits that noise imposes on chemosensing are well characterized for wide concentration ramps (13), typical of laboratory assays and comparable to the gradients generated by large phytoplankton cells, and for intense but short-lived gaussian pulses, mimicking cell lysis events (14, 15). By contrast, our understanding of chemotaxis towards small cells, which may generate gradients tightly confined in space, is rather limited, despite the smallest phytoplankters being by far the most abundant (16, 17). Moreover, while it is qualitatively well understood that chemotaxis can favor bacteria-phytoplankton interactions, it is

Author affiliations: [a]Institute of Environmental Engineering, Department of Civil, Environmental and Geomatic Engineering, ETH Zürich, 8093 Zürich, Switzerland; [b]School of Mathematics and Statistics, The University of Melbourne, Parkville, Victoria, Australia; [c]Univ Rennes, CNRS, IPR (Institut de Physique de Rennes) - UMR 6251, F-35000 Rennes, France

Please provide details of author contributions here.

Please declare any competing interests here.

[1]To whom correspondence should be addressed. E-mail: jonasz.slomka@gmail.com

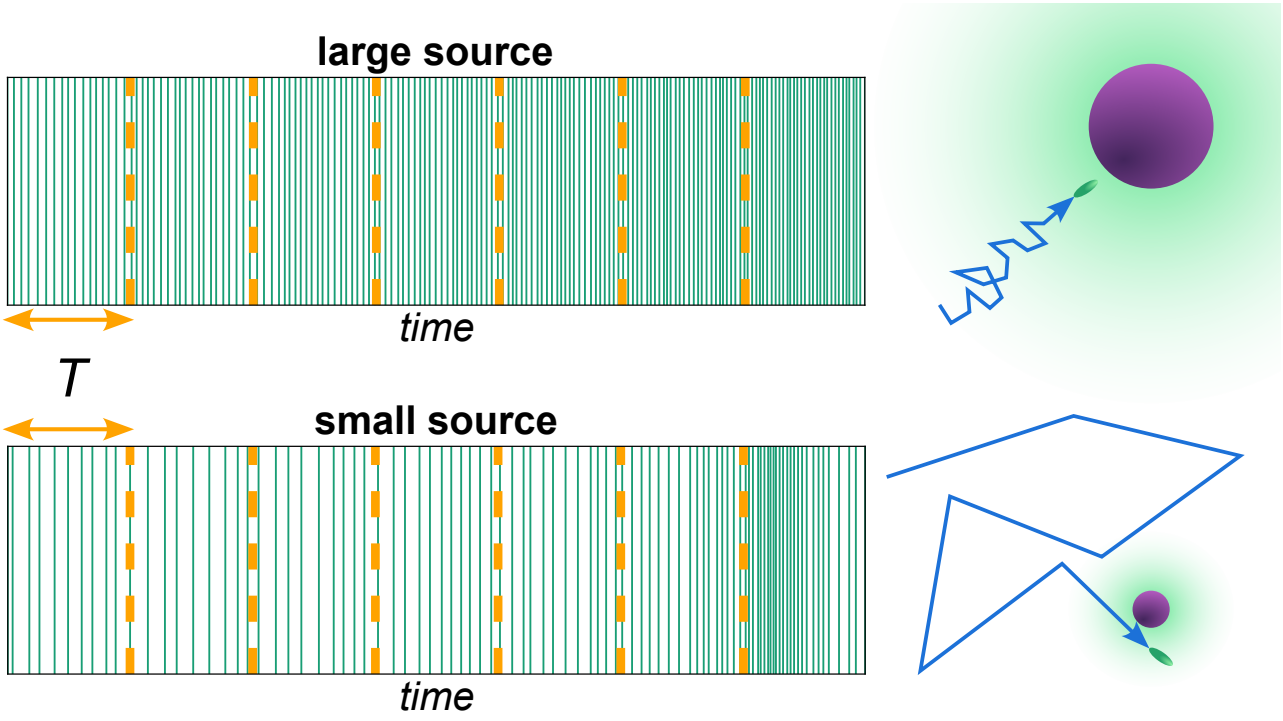

Fig. 1. Detecting chemical gradients to increase encounter rates with phytoplankton through chemotaxis is a size-dependent challenge for bacteria. To estimate the local concentration gradient, the bacterial chemosensory machinery integrates absorption sequences of chemoattractant molecules over a characteristic sensory timescale T. The phytoplankton size determines the lengthscale over which the gradients extend, leading to absorption sequences with well-distinguished features for small and large sources. The limiting factors for the detection of these sources are therefore of different nature: sensing noise for large sources arising from molecular fluctuations and dynamic noise for small sources resulting from bacterial motion and limited temporal resolution.

quantitatively unclear how much interaction rates can increase across the size spectrum.

Here we investigate, through the lens of encounter rates, how chemotaxis can increase interaction rates between bacteria and phytoplankton cells (18). Combining constraints on the detection of noisy and spatially confined gradients with the size-dependent nature of random encounters, we obtain an upper bound on the possible increase in encounter rates resulting from the use of chemotaxis, with respect to purely random searches. Our results, also supported by a numerical model of an ideal sensor, show that chemotaxis towards large phytoplankton cells offers easily accessible but modest reductions in search times; search times for the small picophytoplankton can instead decrease drastically although the risk of failure is high. We hypothesize that such low-risk/low-gain performance for large targets and high-risk/high-gain for small targets may promote size-sensitive chemotactic strategies.

Phytoplankton cells of different sizes generate chemical gradients of varying steepness and spatial extent, posing fundamentally different gradient detection challenges for bacteria (Fig. 1; see also discussion in SI). Bacteria experience concentration fields in the form of temporal sequences of molecular adsorption events, which are integrated over a sensory timescale T to form an estimate of the local concentration gradient (10). When moving in the chemoattractant field generated by a large phytoplankton cell, which may be characterized by wide spatial extent and a shallow gradient, a bacterium will experience a large baseline adsorption rate with only a gradual increase over subsequent sensory windows. Detection can fail if the gradient is too shallow, and the concentration increase is masked by fluctuations in the molecular adsorption events, a scenario which has been modeled in detail before (13). By contrast, in the case of a small phytoplankton cell, whose concentration fields are likely to be weaker and tightly localized in space, the signal will mostly be indistinguishable from the background, until, at very close distance from the phytoplankter, the bacterium will experience a sudden burst in adsorption events localized within a short time interval. Here the limiting factor is not the inherent noise arising from molecular fluctuations, but the dynamic noise resulting from bacterial motion, which limits the ability of the bacteria to properly resolve a signal appearing over timescales comparable or smaller to the sensory timescale T: the limited temporal resolution of the measurements may lead to aliasing effects (), preventing an accurate reconstruction of the gradient. Spatially confined sources have received less attention after Jackson proposed that chemotaxis towards cells smaller than $3 \sim 4\,\mu$m would not be possible (19); recently, however, it was shown that marine bacterium *Marinobacter adhaerens* can use chemotaxis to increase nutrient uptake from the picocyanobacterium *Synechococcus* (20), highlighting how chemotaxis might be relevant even at the smallest scales. To study how the phytoplankton size and the associated sensing limitations affect chemotaxis performance, we next outline how to compute an upper bound on the chemotactic index, a dimensionless number that measures the increase in encounter rate with a phytoplankton cell due to chemotaxis over random motility alone.

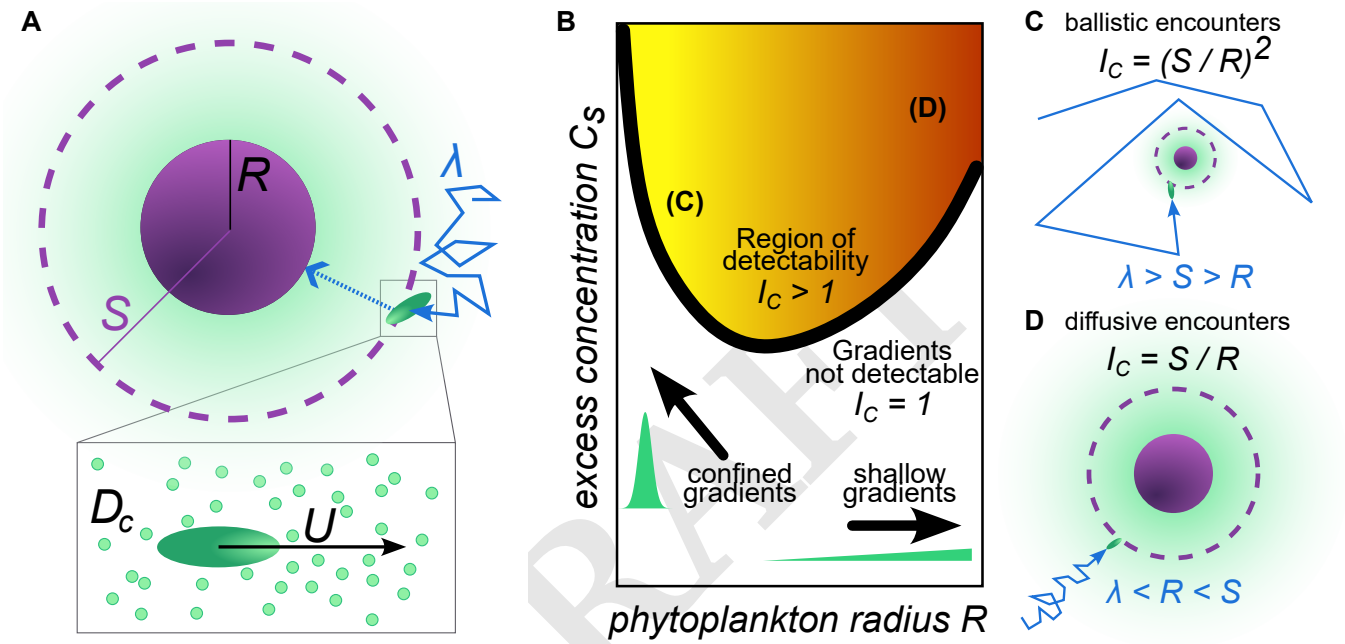

Fig. 2. Chemotactic encounters are limited by the gradients' steepness and spatial extent, and ballistic or diffusive encounters with the sensing horizon. (A) A phytoplankton cell of radius R produces a stationary diffusive field of a chemoattractant, $C(r) = C_0 + C_s R/r$ (represented by the green halo). Far away from the cell, bacteria cannot sense the chemoattractant and thus swim in random walks, with correlation length λ. The "sensory distance" S is the distance from the phytoplankton cell at which a perfect chemotaxer would be able to detect the gradient and encounter its target with a 100% probability. (Inset) Chemosensing is a molecule-counting process based on encounters between the bacterium and individual chemoattractant molecules. Attractant molecules reach the bacterium via diffusion (diffusivity D_c) while the bacterium swims at speed U through the chemoattractant field. (B) Schematic depiction of the performance landscape for chemotactic searches. The source size R and the chemoattractant concentration C_s determine whether gradients can be successfully detected or not. The thick black line defines the boundary of detection, separating the regions where gradient detection is or is not possible. Below the boundary, two conditions limit an organism's ability to perform chemotaxis: gradients are either too spatially confined or too shallow. In this region, chemotaxis provides no benefit over random motility. Above the boundary gradients can be detected, and the increase in encounters compared to random motility, measured by the chemotactic index I_c, is determined by the relationship between bacterial correlation length λ, source size R and sensory radius S. The size dependence of random encounters identifies two subregions within the region of detectability (yellow-red shading), in which the chemotactic index displays two distinct behaviors. Small sources (C) lead to ballistic encounters for which the chemotactic index scales quadratically with the sensory radius S, whereas for large sources (D) the chemotactic index scales only linearly with S due to the diffusive nature of encounters.

We compute an upper bound on the chemotactic index by considering a perfect chemotactic bacterium limited only by random encounters with a sensing horizon - a distance inside which the bacterium detects gradients and flawlessly navigates towards the phytoplankton (Fig. 2). We represent a phytoplankton cell as a sphere of radius R which can exude chemoattractants to generate a diffusive concentration field (see SI for derivation and discussion of other concentration fields)

$$C(r) = C_0 + C_s \frac{R}{r} \quad [1]$$

where C_0 is the background concentration of the compound far away from the phytoplankton cell, C_s is the excess concentration of the compound at the phytoplankton cell surface, and r is the radial distance from the center of the phytoplankton cell ($r \geq R$). In the absence of chemoattractants, a bacterium performs a random walk with speed U and correlation length λ. When chemoattractant gradients are present, the bacterium can bias its motion in the direction of the positive gradient, increasing its chances of encountering a leaking phytoplankton cell. We find an upper bound to the encounter-enhancing effect of chemotaxis by considering the bacterium to be a "perfect chemotaxer": there exists a "sensory horizon", S, around the phytoplankton cell where the bacterium can reliably detect the gradient and exploit it to, eventually, yield an encounter with 100% probability; outside the sensory horizon no chemotactic behavior is manifested (Fig. 2A). The problem of chemotactic encounters with the chemoattractant source is therefore reduced to the problem of identifying the sensory horizon.

The extent of the sensory horizon is defined by the bacterial ability to detect a signal (i.e., a positive gradient) at a given location, as determined by the signal-to-noise ratio. Chemotaxis operates through the adsorption of attractant molecules, which reach the bacterial cell surface with diffusivity D_c (Fig. 2A inset) (10); the swimming speed, U, determines the temporal gradient experienced by the bacterium, $U\nabla C$ (10, 14). In gradients with wide spatial extent, the inherent noise in the gradient measurements, arising from fluctuations in molecular adsorptions, was derived by Mora & Wingreen (13) as $\sigma_0 = \sqrt{3C/(\pi a D_c T^3)}$; at any given location in space (assuming the bacterium is heading straight towards the phytoplankton cell) the signal-to-noise ratio (SNR) is then given by

$$\mathrm{SNR} = \frac{|U\nabla C|}{\sqrt{3C/(\pi a D_c T^3)}}. \quad [2]$$

The SNR quantifies the likelihood to measure a positive gradient: when SNR is high, bacteria have a high probability to detect positive gradients; when it is low, gradients are masked by fluctuations. Eq. (2) assumes that the concentration field does not vary significantly on times shorter than the sensory timescale T, ignoring the contribution of dynamic noise to gradient sensing. ~~We phenomenologically include the dynamic noise contribution by replacing the signal $U\nabla C$ with a discrete approximation $U\nabla_T C$ whichtakes into account the effect of motion during the finite sensory timescale (detailed discussion in SI).~~ It can be shown that introducing a non-linear component to the concentration field (e.g. in the form of a second order expansion) provides a dynamic correction to the noise σ_0 evaluated by Mora and Wingreen, which, for the diffusive field we consider, takes the form

$$\sigma_0^* = \sigma_0 \sqrt{1 + \frac{3}{20}\left(\frac{UT}{R+\Delta r}\right)^2} \quad [3]$$

where Δr is the distance from the surface of the source of radius R. In practice, when the source is small compared the distance traveled by the bacterium during the sensory interval, *and* the bacterium is close to the source, the noise in the gradient estimate increases compared to the case of the linear ramp. Detailed derivation and discussion is provided in the SI. In practice, inclusion of non-linear terms in the computation highlights the importance of movement and size, and effectively introduces a low-pass filter in the sensing process. Since a second order expansion is not sufficient to fully represent the non-linearity of the diffusive concentration field over the entire parameter space, we capture the effect of the dynamic noise by phenomenologically introducting a low-pass filter f, which degrades the SNR for high-frequency signals, without affecting the lower frequency components. The results will be quantiatively, but not qualitatively, sensitive to the exact implementation of this low-pass filter. Further, following Brumley *et al.* (15), we introduce a chemotactic precision factor Π in front of the Mora-Wingreen noise $\sigma = \Pi\sigma_0$, which in marine bacterium *Vibrio anguillarum* was estimated as $\Pi \approx 6$. We then define the sensory horizon S as the farthest distance from the phytoplankton cell at which the SNR overcomes a threshold q; mathematically, S is therefore the solution to the equation

$$\mathrm{SNR} = \frac{|U\nabla C_{(S)}|}{\Pi\sigma_{(S)} f(UT/S)} = \frac{|U\nabla C_{(S)}|}{6\sqrt{\frac{3C_{(S)}}{\pi a D_c T^3}} f(UT/S)} = q. \quad [4]$$

A reasonable choice is $q = 1$, which equates to defining S as the distance where bacteria can detect a positive gradient with a probability $\approx 84\%$ (SI). For any given phytoplankton size and excess concentration, we can then determine whether a sensory horizon exists (i.e., if, for the given parameters, there is a distance $S > R$ at which the SNR overcomes the threshold), and thus gradient detection is possible, or if gradients are not detectable (Fig. 2B). Independently of the details of the signal processing mechanism and of the specific form of the concentration field, the two limiting factors of gradient steepness and spatial confinement, as described by the inherent and dynamic noise respectively, define a convex region where gradients can be detected.

When gradient detection is possible, the performance of chemotactic searches is limited by the ballistic or diffusive nature of encounters with the sensory horizon. In the perfect chemotaxis limit, reaching the sensory horizon S ensures that the bacterium will eventually reach the target phytoplankton: the problem of chemotactic encounters with the phytoplankton cell thus simplifies to the problem of random encounters with the sensory horizon. We quantify the maximum possible performance of a chemotactic search through a chemotactic index, I_c, defined as the ratio between the rate of random encounters with the sensory horizon, S, and the rate of random encounters with the phytoplankton cell of radius R. Successful chemosensing implies an increase in the apparent size of the phytoplankton cell, $S > R$, and is therefore characterized by $I_c > 1$. When a sensory horizon $S > R$ does not exist,

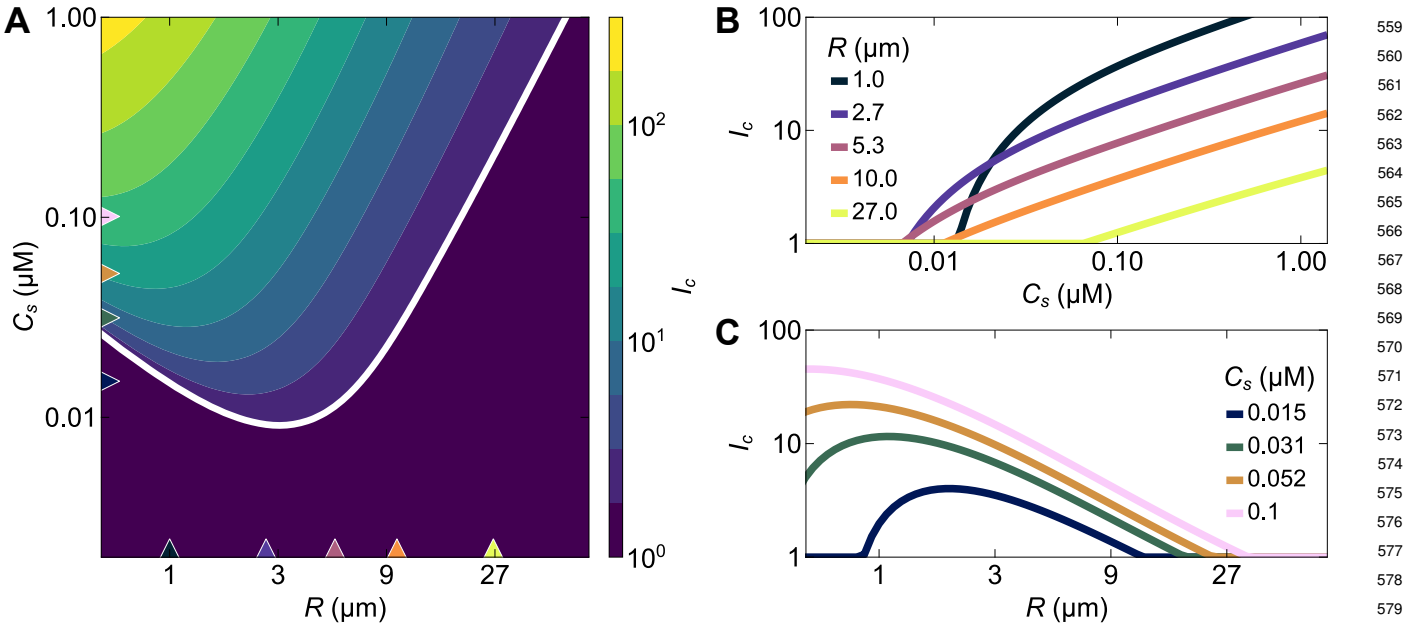

Fig. 3. ~~The stakes are high for encounters with small phytoplankton – the chemotactic index is largest for small phytoplankton, but it drops sharply when gradient detection fails.~~ The stakes are high for encounters with small phytoplankton – the chemotactic index is largest for small phytoplankton, but it drops sharply when gradient detection fails. (A) Performance (I_c) landscape for a bacterium using chemotaxis to drive encounters with spherical targets of different radii (R) and chemoattractant concentrations (C_s) calculated based on Eq. ??. The thick white line defines the boundary of detection, separating the region where gradients are detectable and chemotaxis is beneficial to encounters ($I_c > 1$) from the region where gradients are too shallow or too spatially confined to be detected ($I_c = 1$). (B) Vertical transects from panel A for fixed values of the target radius R (corresponding to the upward-pointing triangles). In chemotaxis towards small targets, a slight variation in the chemoattractant concentration can make the difference between a highly successful search ($I_c \sim 10$) or a failure ($I_c = 1$), whereas for larger targets the dependency of I_c on the chemoattractant concentration is more gradual. (C) Horizontal transects from panel A for fixed values of the chemoattractant concentration C_s (corresponding to the right-pointing triangles). For weak sources, an increase in size R produces initially large enhancements in chemotactic performance, with diminishing returns upon further enlargement. As the source gets stronger, the increase in performance for chemotaxis towards small targets becomes disproportionately larger; larger sources also become detectable although offering modest performance improvements over random searches.

chemotaxis can provide no enhancement to encounter rates and therefore $I_c = 1$ (we ignore possible scenarios where chemotaxis is detrimental to encounters leading to $I_c < 1$).

The chemotactic index, I_c, within the region of detectability is determined (SI) by the relationship between the correlation length of the bacterial random walk, λ, the phytoplankton radius, R, and sensory horizon, S. The encounters with small phytoplankton cells ($\lambda > S > R$) have a ballistic nature and display a quadratic scaling $I_c = S^2/R^2$ (Fig. 2C). For large phytoplankton cells ($\lambda < R < S$) encounters are of diffusive nature and the chemotactic index scales only linearly $I_c = S/R$ (Fig. 2D). The different nature of detection limits and encounter mechanisms for small and large phytoplankton cells suggests an asymmetry in chemotactic performance as a function of size. The asymmetry should be particularly strong at the boundary of detection, where, for large cells, the sensing horizon is comparable with the cell size ($S \sim R$) because gradients are sharpest close to the cell surface. Combined with the linear scaling ($I_c = S/R$), we expect the I_c to vary continuously across the detection boundary for large cells. By contrast, for small cells, the sensing horizon is not limited by gradient sharpness but by the temporal resolution of bacterial measurement, i.e., the sensing horizon is on the order of $S \sim UT$. Consequently, combined with the quadratic scaling ($I_c = S^2/R^2$), we expect I_c to exhibit a sudden jump from $I_c \sim (UT/R)^2$ to $I_c = 1$ across the detection boundary for small cells as we verify next.

Chemotaxis towards small phytoplankton cells can be risky but highly rewarding. Application of our model to a "typical" marine bacterium (radius $a = 0.5\,\mu\text{m}$, swimming speed $U = 50\,\mu\text{m}\,\text{s}^{-1}$, sensory timescale $T = 100\,\text{ms}$) chemotactic towards some sugar-like compound (diffusivity $D_c = 500\,\mu\text{m}^2/\text{s}$) yields a quantitative description of the chemotactic performance landscapes which shows clear differences between the small-radii and the large-radii region (Fig. 3A). Here we assume the background concentration of the compound (C_0 in Equation 1) to be fixed at 1 nM, a value on the low-end for dissolved free amino acids in ocean waters (12). The effect of changing background concentration is discussed in the SI. Contour lines of the I_c profile have a higher density close to the detection boundary in the region of small phytoplankton radii, suggesting that modest variations in the excess concentration C_s leaked by a small phytoplankter can have large impacts on the performance of bacterial chemotaxis. Indeed, the I_c has a much sharper dependency on C_s when the phytoplankton radius R is small, and especially so when crossing the detection boundary (Fig. 3B): while a bacterium might not be able to sense ($I_c = 1$) an attractant gradient from a 1 μm phytoplankter leaking with $C_s = 10\,\text{nM}$, a few nM increase can quickly enhance the I_c to values of 10 and more; as C_s is further increased we get deeper into sensing territory, and the dependency of I_c on C_s quickly smooths out. For larger phytoplankton cells, there is no sharp increase: when the boundary of detection is crossed, the I_c only grows gradually with C_s. Simultaneously, for small values of the excess concentration C_s, an increase in phytoplankton

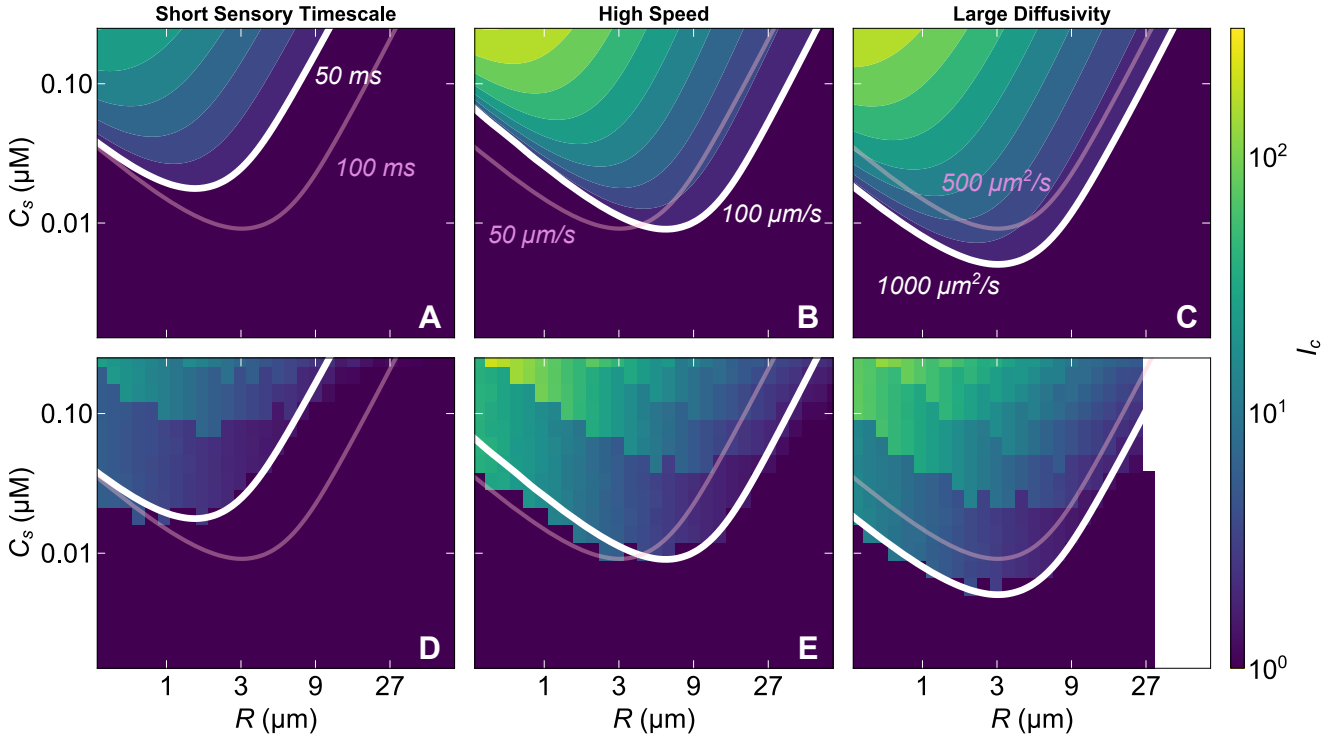

Fig. 4. Bacterial chemotactic strategy controls the chemotactic index but does not alter the high-stakes nature of encounters with small phytoplankton. Performance landscapes of different chemotactic strategies obtained from theoretical (A–C) and computational (D–F) models. In all the panels, the pink curve is the detection boundary for a reference strategy with parameter values $U = 50\,\mu\mathrm{m\,s^{-1}}$, $T = 100\,\mathrm{ms}$, $D_c = 500\,\mu\mathrm{m/s^2}$ (same as in Fig. 3A). (A) Reduction in sensory timescale T from $100\,\mathrm{ms}$ to $50\,\mathrm{ms}$. (B) Increase in swimming speed from $50\,\mu\mathrm{m\,s^{-1}}$ to $100\,\mu\mathrm{m\,s^{-1}}$. (C) Increase in chemoattractant diffusivity from $500\,\mu\mathrm{m^2/s}$ to $1000\,\mu\mathrm{m^2/s}$. (D–F) Theoretically predicted features of bacterial chemotactic performance are reproduced by an ideal sensor based on the Kolmogorov-Smirnov test. In panels D to F, the white line is the detection boundary from the theoretical prediction of panels A to C, respectively. Despite small quantitative differences in the estimated I_c values, arising from the distinct signal processing mechanism and the finite spatial resolution of numerical simulations, the features of the performance landscape are clearly conserved.

radius R leads first to a sharp increase in chemotactic index and then a gradual decrease towards $I_c = 1$ when R overcomes an optimal value (Fig. 3C). As C_s is increased, phytoplankton cells with smaller sizes keep offering disproportionately larger advantages to chemotactic performance compared to the larger cells whose detection requires larger and larger values of C_s.

Variations in chemotactic search strategies, defined by parameters such as swimming speed U, sensory timescale T or diffusivity of the sought-for compound D_c, determine the benefits of chemotaxis for a given phytoplankton radius and excess concentration, but do not affect the fundamental structure of the performance landscape (Fig. 4). A reduction in sensory timescale from 100 to 50 ms significantly decreases bacterial ability to detect gradients from large phytoplankton cells and reduces the overall performance of chemotaxis (Fig. 4A): a larger T reduces sensing noise ($\propto T^{-3/2}$) but increases dynamic noise by reducing the frequency of measurements. An increase in swimming speed from 50 to $100\,\mu\mathrm{m\,s^{-1}}$ improves the performance of chemotaxis within the region of detectability, but the region itself is shifted towards larger radii values, highlighting a tradeoff between degraded spatial resolution (lower frequency of measurements) and improved sensing accuracy by reducing bias in the signal (14)(Fig. 4B). An increase in the diffusivity of the chemoattractant compound from 500 to $1000\,\mu\mathrm{m^2/s}$ (values similar to the diffusion coefficients of sugars and DMSP respectively ()) enhances the signal-to-noise ratio without affecting spatial resolution (sensing noise $\propto D_c^{-1/2}$), and it thus shifts the region of detectability towards lower C_s values (Fig. 4C). Unaffected by the variation in these quantities, the high-stakes nature of chemotactic searches towards small phytoplankton cells is therefore only a direct result of the sharp cutoff on spatial resolution arising from dynamic noise combined with the quadratic scaling of the I_c associated to ballistic encounters.

The generality of our theoretical analysis is supported by a minimal numerical model of an ideal sensor ~~which has no direct relationship to bacterial chemosensory mechanisms~~ (Fig. 4D–F). This ideal sensor is defined as a sphere moving at constant speed U towards a phytoplankton cell leaking a chemoattractant field $C(r)$. As it moves, the sensor registers all the adsorption events of chemoattractant molecules, occurring as Poisson events with instantaneous rate $4\pi D_c a C(r)$, where r is the instantaneous position of the sensor. After an interval of length T, the registered events are processed and a new acquisition starts. For the signal processing, the sensor performs a one-sided Kolmogorov-Smirnov test (21) comparing the distribution of the waiting times recorded in the first and the second half of the acquisition window. If the cumulative distribution function in the second half is found to be larger than that in the first half, then the sensor has detected a gradient. Averaging the successful gradient detections over an ensemble ($N = 1000$) of such ideal sensors provides an estimate of the sensory distance S, defined as the largest distance where at least a fraction f of the sensors has detected

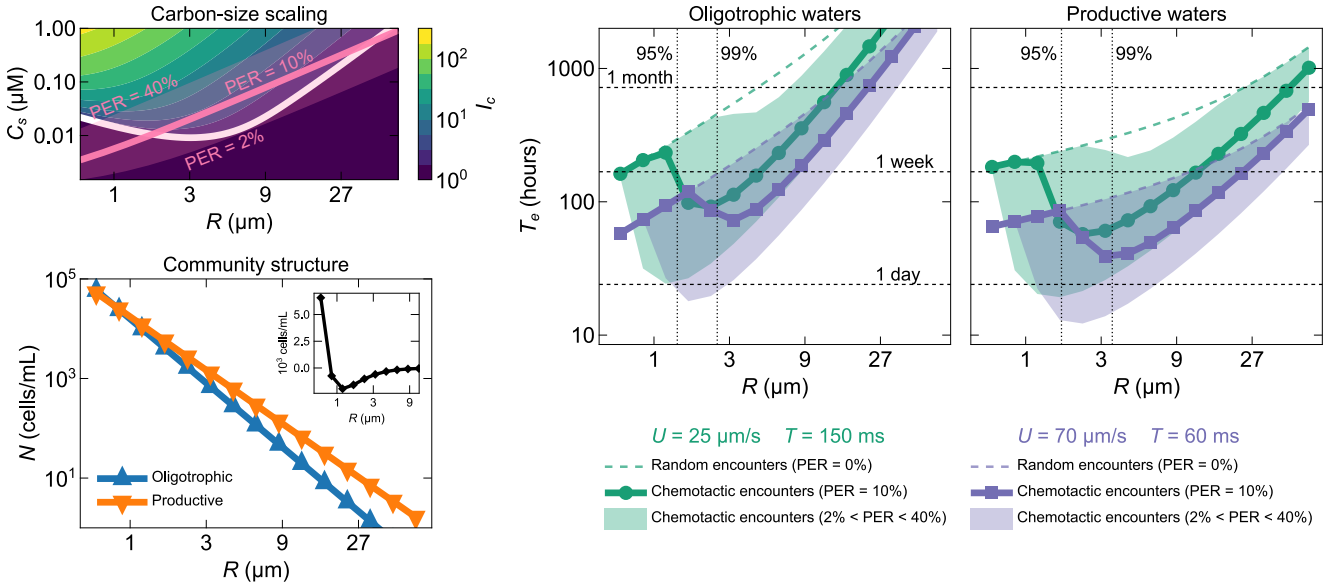

Fig. 5. The high-stakes nature of phytoplankton-bacteria interactions may promote a diversity of chemotactic strategies. (A) Characteristic values of size and released chemoattractant for phytoplankton cells are constrained by carbon-size scaling laws (pink areas). When overlaid on the performance landscape of a bacterium (same as in Fig. 3A), the physiological range of exudation rates lies across the boundary of detection. The thick pink line corresponds to phytoplankton cells with a percent extracellular release (PER) of 10%, the shaded pink band represents variations in the percent extracellular release between 2% (lower limit) and 50% (upper limit). (B) Marine phytoplankton communities are dominated by small cells. The size structure follows a power-law distribution, where the abundance N decreases with increasing size R as $N(R) \propto R^{-3\alpha}$. The allometric exponent is larger in oligotrophic waters ($\alpha \simeq 0.9$) than in more productive waters ($\alpha \simeq 0.75$). Both communities are normalized to a total cell abundance of 1×10^5 cells/mL. Inset: difference between cell abundance in oligotrophic and productive waters. (C-D) Comparison of search times between random motility and chemotaxis. Carbon-size scaling, phytoplankton community structure and chemotactic index jointly define the average search time (T_e) (Eq. 5) an individual bacterium requires to encounter a phytoplankton cell using chemotaxis. The thin broken lines represent the search times in the absence of chemotaxis ($I_c = 1$). The thick lines with markers indicate search times for phytoplankton cells with percent extracellular release of 10% (corresponding to the thick pink line in panel A), and the shaded bands represent variations in percent extracellular release between 2% and 50% (matching the pink shaded band in panel A). The two curves correspond to distinct chemotactic strategies: in green with circle markers, a strategy with low speed and long sensory timescale; in violet with square markers, a strategy with high swimming speed and short sensory timescale. The vertical dotted lines mark the radii corresponding to the 95th and 99th percentiles of the phytoplankton community abundance.

a gradient. The estimates of S can then be used to evaluate the chemotactic index I_c. Remarkably, we find that choosing a high consensus threshold $f = 0.99$ provides close agreement with our theoretical calculations, both in terms of the shape of the detectability region and of the estimated I_c values. This fact highlights how the detection limits evaluated for bacterial chemosensing and the asymmetric nature of the chemotactic performance are not specific to bacteria, but can be used to describe a wide class of systems estimating gradients through temporal comparisons, independently of the particular signal processing mechanism and navigation parameters.

The physiological range of exudation rates for healthy phytoplankton cells lies across the boundary of chemotactic detection (Fig. 5A), suggesting that chemotaxis might play a relevant role for encounters across the entire size spectrum. The physiology of marine phytoplankton enforces a specific coupling between size R and excess concentration C_s. Empirical carbon-size scaling laws predict that the carbon content of a cell scales with cell size as $\sim R^{2.28}$ (22); the percent extracellular release (PER) then determines how much of this total content is leaked to the environment (SI). Average values of the PER are expected to be around 10%, but variations between values of PER $\approx$ 2% and 40% are typical and also strongly dependent on physiological and environmental conditions (23).

The steep size-structure of marine phytoplankton communities favors encounters with small phytoplankton cells. The average search time required by an individual bacterium to encounter a phytoplankton cell can be obtained as

$$T_e = \frac{1}{I_c \Gamma N} \qquad [5]$$

where N is the phytoplankton concentration, and Γ is the random encounter kernel~~between the bacterium and the phytoplankton and N is the phytoplankton concentration~~, which represents the amount of volume swept, per unit time, by the motion of the bacterium relative to the phytoplankton cell (18, 24). Marine phytoplankton communities have characteristic size structures which usually follow a power-law size-abundance relationship of the form $N(R) \propto R^{-3\alpha}$, where the allometric exponent α takes typical values $\alpha \approx 0.9$ in oligotrophic waters and $\alpha \approx 0.75$ in productive waters (17). Phytoplankton cells with smaller radii are therefore vastly more abundant than cells with larger radii, and particularly so in oligotrophic environments where large phytoplankters are extremely rare (Fig. 5B). This ~~peculiar~~ steep size-structure allows bacterial search times for small phytoplankton cells to be much shorter than those for larger cells. The overabundance of small cells, combined with the asymmetric performance landscape of bacterial chemotaxis, further raises the stakes for chemotactic searches in the low end of the size spectrum.

Chemotaxis significantly reduces search times in the sub-5 μm range, but different chemotactic strategies can display dramatic performance differences in the low end of the spectrum (Fig. 5C–D). In the absence of chemotaxis, small phytoplankton cells require much shorter search times than

large phytoplankton (Fig. 5C–D, thin broken lines). In oligotrophic waters, a bacterium swimming randomly with speed $40\,\mu m\,s^{-1}$ can encounter a phytoplankton of radius $0.5 \sim 0.7\,\mu m$ roughly every 100 hours, while encountering a phytoplankton in the range ~~24 ∼ 33 µm~~ 24—33 µm will take on average more than a month. In productive waters the search times for small cells are only slightly higher, whereas those for larger cells fall down below a month. Bacteria with a higher swimming speed of $80\,\mu m\,s^{-1}$ reduce their random search times due to improved exploration efficiency, although that comes with a tradeoff in terms of chemotactic performance, as also shown in Fig. 4B. The decreases in search times resulting from the use of chemotaxis, over the whole range of phytoplankton PER values, are shown as shaded bands in Fig. 5C and D, with the thick marker-decorated line representing the typical value PER = 10%. Bacteria with lower speed but longer sensory timescales T can decrease their search times for the smallest phytoplankton almost by a factor 10, whereas the faster swimming bacteria with a shorter sensory timescale cannot benefit at all from chemotaxis at this extreme of the spectrum. While the major difference in the I_c between the two strategies is limited to the micron-size range, we stress that this region of the size-spectrum encloses the vast majority of the population. The 95th percentile of the populations (marked by the dotted vertical lines in the figures) is below the 2 µm radius, and, in both environments, more than half of the population is contained within the first size class. Therefore, losing the ability to increase encounters with the smallest cells in the spectrum can dramatically impact the dynamics and the fate of populations. We must also note that the boost in chemotactic performance towards small cells occurs only at high PER, while no gain can be obtained with intermediate PER values; for the larger ($> 2\,\mu m$) radii, the reduction in search times is more robust and occurs also at lower PER values.

Assuming the minimization of search times to be the end-goal of a cell, it is suggestive to think of the chemotactic encounter problem as an evolutionary game with a strongly asymmetric fitness function. In this context, the I_c can be interpreted as a measure of the maximum possible fitness attainable by a bacterium: it is possible to obtain huge fitness benefits in the search for small phytoplankton cells, but relatively small ones when searching for large cells. We must keep in mind, however, that the encounter is only the initiating step of a possibly multi-stage interaction process and that fitness is determined by the ability to grow and reproduce. To obtain a more complete eco-evolutionary picture, one would need to simultaneously consider the search time and the growth return associated to phytoplankton cells of different sizes. In fact, chemotaxis is expected to not only reduce search times, but to also (and most prominently) improve the growth returns, allowing bacteria to remain nearby local maxima of chemoattractants even without a direct encounter (25). Indeed, Raina *et al.* (20) have shown that *Marinobacter adhaerens* can use chemotaxis to increase nutrient uptake ~~(and therefore growth returns)~~ from *Synechococcus* cells, ~~but they don't provide any information on whether chemotaxis also reduces the search times~~and also increase the encounter rates with their phycosphere. ~~Further considerations~~ Generally, it can be expected that larger sources, while offering less drastic enhancements to search times, may provide larger growth returns, but any further consideration on the growth returns should also include estimates of the energy expenditure associated with motility and chemotaxis (26, 27), and the fact that foraging efficiency is typically positively correlated with predation risk ~~(28)~~(28, 29).

~~Our work points to several potential extensions to better understand the role of chemotaxis in regulating encounters. The requirement to include multiple phenomena in our model (bacterial motility, dynamic and inherent noise in chemosensing, phytoplankton exudation, carbon-size scalings, community structures) clearly leads to simplifications which complicate the task of making explicit predictions, but our approach provides at least a framework in which the effects of chemotaxis on microscale interactionscan be better understood.~~ Even in our limited framework, the strong sensitivity of the chemotactic performance to a large variety of parameters, such as swimming speed, size, leakage rates, molecular diffusivity, sensory timescales and chemotactic sensitivity, paints a complex landscape. While our approach allowed us to identify general features of chemotactic searches, it also highlighted that it is not possible to unambiguously define a universal limit to chemotactic sensing, as ambitiously attempted by Jackson almost 40 years ago (19). Rather, our theoretical results, in combination with modern experimental efforts, namely the already mentioned *Marinobacter adhaerens*—*Synechococcus* interaction (20), or the recent investigation of the chemotactic response of marine heterotrophic bacteria to the exudates of virus-infected *Synechococcus* extending to distances larger than 100 µm (30), strongly suggest that, while chemotaxis may be more pervasive than previously thought, outstanding questions related to its operational limits or its benefit to cell growth, may need to be answered individually for each specific system.

This incredibly intricate picture can be further enriched by considering the environmental, physiological and behavioral changes to which bacteria and phytoplankton cells can be exposed throughout their lives. Phytoplankton exudates typically vary in composition and abundance as a function of the organism's physiological state and life stage (4, 6, 23) ; different chemoattractants (which we only considered through their diffusivity) are known to elicit wildly different chemotactic responses, especially when multiple chemical species are simultaneously present (31), and each of them may affect bacterial metabolism in different ways (). Metabolic shifts can in turn result in dramatic variations of the chemotactic sensitivity (), thus affecting the interaction rates with the phytoplankton cells and introducing feedback loops between behavior, physiology, and environment. All these factors and many others (fluid flows (32–35), predation (28) , fluctuations from the scale of minutes, to days, to seasonal cycles (36–38)) contribute to shape the microscale interaction landscape of the ocean in a way that, as a whole, is still beyond the reach of our theoretical models and experimental capabilities. Despite many invaluable contributions to these subjects in the literature of the last four decades, our understanding of the mechanisms through which chemotaxis regulates microscale interactions, and their pervasiveness and consequences, are, clearly, still at an embryonal stage (39).

Explicit numerical simulations of ~~chemotactic bacteria~~ bacterial chemotaxis towards leaky phytoplankton cells could

also help establish relationships help establish relationsihps between search times and uptake rates, and how these two quantities processes are simultaneously modulated by motile and chemotactic properties across the size spectrum. Recent results on the competitive effect of Tar and Tsr receptors on chemotaxis towards the model attractants aspartate and serine (40) could help develop more sophisticated models to better describe chemotactic navigation in complex multi-species chemical landscapes. Different chemoattractants (which we only considered through their molecular diffusivity) are also known to elicit wildly different chemotactic responses, especially when multiple chemical species are simultaneously present (31), an effect which we are not able to include in our calculations. Moreover, there is a clear need to design experiments to assess , how far from a phytoplankton cell chemoattractants can be detected, and, at least in simple scenarios with single chemical species, how close to these the predicted theoretical limits bacteria can operateand if it is reasonable to tie the mathematical concept of the sensory horizonto the empirical notion ; such experiments could aid in providing a stronger connection between the mathematical notion of "sensory horizon" that we introduced in this work, and the empirically grounded concept of phycosphere (6, 41, 42). , the biochemically-rich microenvironment which surrounds phytoplankton cells.

Using idealized models of phytoplankton leakage and bacterial chemotaxis, we calculated upper bounds on the enhancement in bacteria-phytoplankton encounters driven by chemotaxis over random motility, and studied how sensitive the enhancement is to the size of phytoplankton. We found that bacterial chemotaxis offers low-risk/low-gain performance for searches of large phytoplankton but high-risk/high-gain performance for small phytoplankton. These tradeoffs arise from chemotactic encounters being limited by fundamentally different mechanisms at the two ends of phytoplankton size spectrum. For large cells, the limitation stems from gradients' steepness and the diffusive nature of bacterial motility and leads to a moderate reduction in chemotactic search times. By contrast, for small phytoplankton, the limit is set by the gradients' spatial confinement and ballistic motility of bacteria, which, in principle, allows for nearly ten-fold reductions in search times provided that bacteria can detect the gradients. We found that searching for small phytoplankton is more efficient when bacteria swim slower but integrate the gradients over longer sensory timescales. Overall, our results suggest that the high-stakes nature of encounters with small phytoplankton is a fundamental feature of chemotactic searches that may drive a diversity of size-sensitive chemotactic strategies.

Author Affiliations. Include department, institution, and complete address, with the ZIP/postal code, for each author. Use lowercase letters to match authors with institutions, as shown in the example. PNAS strongly encourages authors to supply an ORCID identifier for each author. Individual authors must link their ORCID account to their PNAS account at www.pnascentral.org. For proper authentication, authors must provide their ORCID at submission and are not permitted to add ORCIDs on proofs.

Digital Figures. EPS, high-resolution PDF, and PowerPoint are preferred formats for figures that will be used in the main manuscript. Authors may submit PRC or U3D files for 3D images; these must be accompanied by 2D representations in TIFF, EPS, or high-resolution PDF format. Color images must be in RGB (red, green, blue) mode. Include the font files for any text.

Images must be provided at final size, preferably 1 column width (8.7cm). Figures wider than 1 column should be sized to 11.4cm or 17.8cm wide. Numbers, letters, and symbols should be no smaller than 6 points (2mm) and no larger than 12 points (6mm) after reduction and must be consistent.

Supporting Information Appendix (SI). Authors should submit SI as a single separate SI Appendix PDF file, combining all text, figures, tables, movie legends, and SI references. SI will be published as provided by the authors; it will not be edited or composed. Additional details can be found in the PNAS Author Center. The PNAS Overleaf SI template can be found here. Refer to the SI Appendix in the manuscript at an appropriate point in the text. Number supporting figures and tables starting with S1, S2, etc.

Authors who place detailed materials and methods in an SI Appendix must provide sufficient detail in the main text methods to enable a reader to follow the logic of the procedures and results and also must reference the SI methods. If a paper is fundamentally a study of a new method or technique, then the methods must be described completely in the main text.

Materials and Methods

All the data shown in this work has been generated through custom Julia () code; all the processed data and the scripts used to generate it are freely available at zenodo and github respectively. Project codes and data were managed with DrWatson.jl (), explicit simulations of molecular absorption events made use of Distributions.jl (), and HypothesisTests.jl () was employed to perform the Kolmogorov-Smirnov tests. Figures were realized with Makie.jl () and Inkscape ().

ACKNOWLEDGMENTS. R.F. acknowledges funding from the European Union's Horizon 2020 research and innovation programme under Marie Skłodowska-Curie grant no. 955910. R.S. acknowledges... J.S. acknowledges funding from Swiss National Science Foundation Ambizione grant no. `PZ00P2_202188`. We also gratefully acknowledge ETH Zürich (Euler cluster) for providing computational resources.

1. F Azam, Microbial Control of Oceanic Carbon Flux: The Plot Thickens. *Science* **280**, 694–696 (1998).
2. JB Raina, V Fernandez, B Lambert, R Stocker, JR Seymour, The role of microbial motility and chemotaxis in symbiosis. *Nat. Rev. Microbiol.* **17**, 284–294 (2019).
3. JB Raina, et al., Chemotaxis shapes the microscale organization of the ocean's microbiome. *Nature* (2022).
4. DC Thornton, Dissolved organic matter (DOM) release by phytoplankton in the contemporary and future ocean. *Eur. J. Phycol.* **49**, 20–46 (2014).
5. S Smriga, VI Fernandez, JG Mitchell, R Stocker, Chemotaxis toward phytoplankton drives organic matter partitioning among marine bacteria. *Proc. Natl. Acad. Sci. USA* **113**, 1576–1581 (2016).
6. JR Seymour, SA Amin, JB Raina, R Stocker, Zooming in on the phycosphere: The ecological interface for phytoplankton–bacteria relationships. *Nat. Microbiol.* **2**, 17065 (2017).
7. JM Sieburth, V Smetacek, J Lenz, Pelagic ecosystem structure: Heterotrophic compartments of the plankton and their relationship to plankton size fractions 1. *Limnol. Ocean.* **23**, 1256–1263 (1978).
8. RM Macnab, DE Koshland, The Gradient-Sensing Mechanism in Bacterial Chemotaxis. *Proc. Natl. Acad. Sci. USA* **69**, 2509–2512 (1972).
9. DA Brown, HC Berg, Temporal Stimulation of Chemotaxis in *Escherichia coli*. *Proc. Natl. Acad. Sci. USA* **71**, 1388–1392 (1974).
10. H Berg, E Purcell, Physics of chemoreception. *Biophys. J.* **20**, 193–219 (1977).
11. PR ten Wolde, NB Becker, TE Ouldridge, A Mugler, Fundamental Limits to Cellular Sensing. *J. Stat. Phys.* **162**, 1395–1424 (2016).
12. C Lee, JL Bada, Amino acids in equatorial Pacific Ocean water. *Earth Planet. Sci. Lett.* **26**, 61–68 (1975).

13. T Mora, NS Wingreen, Limits of Sensing Temporal Concentration Changes by Single Cells. *Phys. Rev. Lett.* **104**, 248101 (2010).
14. AM Hein, DR Brumley, F Carrara, R Stocker, SA Levin, Physical limits on bacterial navigation in dynamic environments. *J. R. Soc. Interface* **13**, 20150844 (2016).
15. DR Brumley, et al., Bacteria push the limits of chemotactic precision to navigate dynamic chemical gradients. *Proc. Natl. Acad. Sci. USA* **116**, 10792–10797 (2019).
16. WG Sprules, M Munawar, Plankton Size Spectra in Relation to Ecosystem Productivity, Size, and Perturbation. *Can. J. Fish. Aquat. Sci.* **43**, 1789–1794 (1986).
17. P Cermeño, F Figueiras, Species richness and cell-size distribution: Size structure of phytoplankton communities. *Mar. Ecol. Prog. Ser.* **357**, 79–85 (2008).
18. J Słomka, et al., Encounter rates prime interactions between microorganisms. *Interface Focus.* **13**, 20220059 (2023).
19. GA Jackson, Simulating chemosensory responses of marine microorganisms: Bacterial chemokinesis. *Limnol. Ocean.* **32**, 1253–1266 (1987).
20. JB Raina, et al., Chemotaxis increases metabolic exchanges between marine picophytoplankton and heterotrophic bacteria. *Nat. Microbiol.* **8**, 510–521 (2023).
21. FJ Massey, The Kolmogorov-Smirnov Test for Goodness of Fit. *J. Am. Stat. Assoc.* **46**, 68–78 (1951).
22. MM Mullin, PR Sloan, RW Eppley, Relationship between Carbon Content, Cell Volume, and Area in Phytoplankton. *Limnol. Ocean.* **11**, 307–311 (1966).
23. E Marañón, P Cermeño, E Fernández, J Rodríguez, L Zabala, Significance and mechanisms of photosynthetic production of dissolved organic carbon in a coastal eutrophic ecosystem. *Limnol. Ocean.* **49**, 1652–1666 (2004).
24. T Kiørboe, *A Mechanistic Approach to Plankton Ecology*. (Princeton University Press, Princeton), (2008).
25. VI Fernandez, Y Yawata, R Stocker, A Foraging Mandala for Aquatic Microorganisms. *ISME J.* **13**, 563–575 (2019).
26. G Malaguti, PR ten Wolde, Theory for the optimal detection of time-varying signals in cellular sensing systems. *eLife* **10**, e62574 (2021).
27. JM Keegstra, F Carrara, R Stocker, The ecological roles of bacterial chemotaxis. *Nat. Rev. Microbiol.* (2022).
28. LT Nielsen, T Kiørboe, Foraging trade-offs, flagellar arrangements, and flow architecture of planktonic protists. *Proc. Natl. Acad. Sci. USA* **118**, e2009930118 (2021).
29. A Ebrahimi, A Goyal, OX Cordero, Particle foraging strategies promote microbial diversity in marine environments. *eLife* **11**, e73948 (2022).
30. RJ Henshaw, et al., Early viral infection of cyanobacteria drives bacterial chemotaxis in the oceans, (Biophysics), Preprint (2023).
31. EE Clerc, et al., Strong chemotaxis by marine bacteria towards polysaccharides is enhanced by the abundant organosulfur compound DMSP. *Nat. Commun.* **14**, 8080 (2023).
32. JD Bowen, KD Stolzenbach, SW Chisholm, Simulating bacterial clustering around phytoplankton cells in a turbulent ocean. *Limnol. Ocean.* **38**, 36–51 (1993).
33. N Blackburn, T Fenchel, Influence of bacteria, diffusion and shear on micro-scale nutrient patches, and implications for bacterial chemotaxis. *Mar. Ecol. Prog. Ser.* **189**, 1–7 (1999).
34. T Kiørboe, GA Jackson, Marine snow, organic solute plumes, and optimal chemosensory behavior of bacteria. *Limnol. Ocean.* **46**, 1309–1318 (2001).
35. JR Taylor, R Stocker, Trade-Offs of Chemotactic Foraging in Turbulent Water. *Science* **338**, 675–679 (2012).
36. JR Bernhardt, MI O'Connor, JM Sunday, A Gonzalez, Life in fluctuating environments. *Phil. Trans. R. Soc. B* **375**, 20190454 (2020).
37. O Karin, U Alon, Temporal fluctuations in chemotaxis gain implement a simulated-tempering strategy for efficient navigation in complex environments. *iScience* **24**, 102796 (2021).
38. J Nguyen, J Lara-Gutiérrez, R Stocker, Environmental fluctuations and their effects on microbial communities, populations and individuals. *FEMS Microbiol. Rev.* **45**, fuaa068 (2021).
39. JR Seymour, DR Brumley, R Stocker, JB Raina, Swimming towards each other: The role of chemotaxis in bacterial interactions. *Trends Microbiol.* p. S0966842X23003608 (2024).
40. L Li, et al., Phenotypic Variability Shapes Bacterial Responses to Opposing Gradients. *PRX Life* **2**, 013001 (2024).
41. W Bell, R Mitchell, CHEMOTACTIC AND GROWTH RESPONSES OF MARINE BACTERIA TO ALGAL EXTRACELLULAR PRODUCTS. *Biol. Bull.* **143**, 265–277 (1972).
42. AJ Platt, KE Whalen, Probing the Phycosphere: Techniques to Study Bacteria-Phytoplankton Interactions. *Integr. Comp. Biol.* p. icad065 (2023).